COMPARISON OF 1-D EJECTOR MODELLING APPROACH AND COMPUTATIONAL FLUID DYNAMICS (CFD) SIMULATION TO PREDICT THE PERFORMANCE OF EJECTOR DEVICES

Nikolaos E. Karkalos[1], Konstantinos Braimakis[2,*], Angelos P. Markopoulos[3], Aris-Dimitrios Leontaritis[1], Sotirios Karellas[1]

[1]Laboratory of Thermal Processes, School of Mechanical Engineering, National Technical University of Athens, Athens, Greece
[2]Laboratory of Refrigeration, Air-Conditioning & Solar Energy, School of Mechanical Engineering, National Technical University of Athens, Athens, Greece
[3]Laboratory of Manufacturing Technology, School of Mechanical Engineering, National Technical University of Athens, Athens, Greece

*Corresponding Author: mpraim@central.ntua.gr

ABSTRACT

The goal of the present work is to perform a comparison of the numerical simulation results obtained by a 1-D model and CFD-based 2-D models regarding the preliminary study of the operation and performance of an ejector device used in an ejector cooling cycle (ECC) which is a part of a trigeneration prototype intended for vessel engine waste heat recovery (WHR), being developed in the context of the ZHENIT H2020 project. While 1-D ejector models have been demonstrated to accurately predict their performance for particular cases and can be used in the calculation of main ejector dimensions, they employ simplifying assumptions and often involve the use of empirical correlations, the validity of which is restricted to specific working fluids and operating conditions. Furthermore, 1-D models do not take into account a large number of secondary but important ejector geometric parameters. Therefore, in the case that experimental data are not directly available, cross validation of their results with those obtained through the use of more sophisticated CFD-based approaches can provide a valuable tool for the evaluation of their accuracy. The ECC which provides the basis for the investigated ejector geometry operates with working fluid R1233zd(E). According to the nominal operating conditions, the primary flow enters the ejector inlet at relatively high temperature of 130°C(5 K superheating) and is used for the entrainment of low-pressure vapor leaving the cooling evaporator at 12°C (5 K superheating).Two ejector geometries are evaluated, featuring different nozzle exit position (NXP) values. The comparative assessment of the two modelling approaches reveals that there are substantial deviations between their outcome, especially regarding the secondary inlet mass flow rate and ejector entrainment ratio, suggesting that necessary adjustments are required for the 1-D model to provide accurate results under the investigated conditions.

1 INTRODUCTION

Ejector devices utilize the energy of a high-pressure motive fluid to entrain and compress a low-pressure fluid to a final intermediate discharge pressure (Besagni, Mereu, & Inzoli, 2016; Braimakis, 2021).They are usually classified based on three main characteristics; the nozzle position and design, as well as the number of fluid phases in the inlets and outlet of the ejector (Elbel & Hrnjak, 2008). For example, if the nozzle exit is positioned inside the suction chamber, a constant pressure mixing ejector configuration exists, while the configuration including the nozzle exit in the constant-area section, a constant-area mixing ejector is created, with different expected performance from the former configuration (Besagni et al., 2016; Tashtoush, Al-Nimr, & Khasawneh, 2019).

https://doi.org/10.52202/077185-0166

Ejectors are often studied as components of ejector cooling cycles (ECC), which can be deployed as alternatives to vapor compression cycles in order to utilize waste heat or solar thermal energy to produce cooling with very low consumption of electrical energy. Their main advantages include simple and compact design, relatively low operating and maintenance costs and lack of moving parts, with relatively long life and minimal vibrations (Ma, Zhang, Li, & Riffat, 2019; Van den Berghe, Dias, Bartosiewicz, & Mendez, 2023; Yadav, Murari Pandey, & Gupta, 2021).

Given the great impact of ejector performance in the overall performance of ECCs, it is necessary to understand the related thermal and flow phenomena occurring during their operation to predict the performance of new designs and optimize their efficiency to maximize their potential for different applications, especially when relevant experimental data are not available, a common situation when novel working fluids and/or application settings are considered. Several simple ejector modeling approaches have been proposed, with 1-D models being attractive thanks to their negligible computational cost, which makes them suitable for optimization purposes (Besagni, Mereu, Chiesa, & Inzoli, 2015; Riffat, Jiang, & Gan, 2005). 1-D models can be either based on simplified numerical solution of 1-D flow equations(Van den Berghe, Dias, et al., 2023)or analytical ideal gas law expressions which describe the fluid flow in ejectors (Besagni et al., 2015; Park & Kang, 2023). Some common features of 1-D models include the assumption of steady flow and constant thermophysical properties, the use of ideal gas equations and the neglection of gravity and isentropic conditions, among others (Shi et al., 2015; Song, Ma, Wang, Yin, & Cao, 2020). These can give rise to perceptible deviations from experimental findings. Even though attempts for improved 1-D models exist(Park & Kang, 2023; Van den Berghe, Bartosiewicz, & Mendez, 2023), the limitations of these models can restrict their reliable use when novel cooling fluids are employed, especially in conditions different from which the existing empirical coefficients for ejector performance were derived.

Contrary to 1-D models, CFD models entail a higher computational cost, but can provide a substantially deeper insight into the physical mechanisms of ejector operation after appropriate validation by available experimental data(Croquer, Poncet, & Galanis, 2016).Up to date, very few studies have attempted to provide a direct comparison between the 1-D and 2-D CFD models for ejectors used in ECCs. Addressing this gap, in the present work, a comparative assessment regarding the prediction of mass flow rate and entrainment ratio for two different ejector geometries by a 1-D and 2-D CFD models (pure 2-D and axisymmetric) is attempted. This work is expected to yield valuable conclusions regarding the capabilities of the two types of models and suggest possible ways to develop a reliable predictive model for the optimization of ejector performance.

2 METHODOLOGY

2.1 Overview

As it was previously discussed, the goal of the present study is the comparison of the ejector operation numerical simulation results obtained through a 1-D model and CFD 2-D models. The most important parameter of an ejector device is the entrainment ratio (ω), which is equal to the ratio of the secondary ($\dot{m}_s$) to primary ($\dot{m}_p$) flow mass flow rates:

$$\omega = \frac{\dot{m}_s}{\dot{m}_p} \tag{1}$$

Essentially, the higher the entrainment ratio, the better the performance of the ejector, as more low-pressure fluid can be entrained for mass unit of high-pressure primary fluid, resulting in higher thermal COP values. Because of its significance, the entrainment ratio will be used as a key performance metric for the comparison of the 1-D and CFD 2-D models. It should be noted that due to the fact that no experimental results are yet available from the real facility, this work is relevant to the evaluation of the capabilities of the two types of models and the comparison of their results in order to verify the extent of their deviations. In the following sections, the 1-D and CFD 2-D modelling approaches are presented.

2.2 Ejector geometry

Ejectors are composed of three distinct sections: the converging-diverging nozzle (CDN), the constant area section (CAS) and the diffuser. Their design is defined by several geometric parameters involving various cross-sectional flow areas, lengths, and angles, as shown in Figure 1. In the present work, the

 https://doi.org/10.52202/077185-0166

ejector geometry was derived based on the specifications of an ECC that is part of an Organic Rankine Cycle – hybrid Ejector-Vapor Compression Cycle (EVCC) for the production of electricity, heating and cooling through the utilization of vessel engine waste heat, currently being developed in the context of the ZHENIT H2020 project. The design specifications of the application are summarized in Table 1. It is noted that the nominal thermal input to the ECC is about 10 kWth, while the driving heat temperature is 140°C.

Table 1 ECC design specifications

Parameter	**Value**
Working fluid	R1233zd(E)
Primary flow mass flow rate (kg/s)	0.045
Primary flow pressure (bar)	17.35
Primary flow temperature (°C)	130 (5 K superheating)
Secondary flow pressure (bar)	0.65
Secondary flow temperature (°C)	12 (5 K superheating)
Condensation temperature (°C)	42.7
Condensation pressure (bar)	2.35

The CDN throat and outlet diameters (d_t and d_1) and the CAS diameter (d_{CAS}) were determined according to the simulation results of the 1-D model that is used in the present work. All additional geometric parameters were determined following the findings of theoretical and experimental studies (Chen, Jin, Shimizu, Hihara, & Dang, 2017; Huang, Chang, Wang, & Petrenko, 1999; Shestopalov, Huang, Petrenko, & Volovyk, 2015) along with recommendations by ESDU (ESDU, 1984, 1986, 1992) that were compiled in the study by Sanaye et al. (Sanaye, Farvizi, Refahi, & Rafieinejad, 2019).

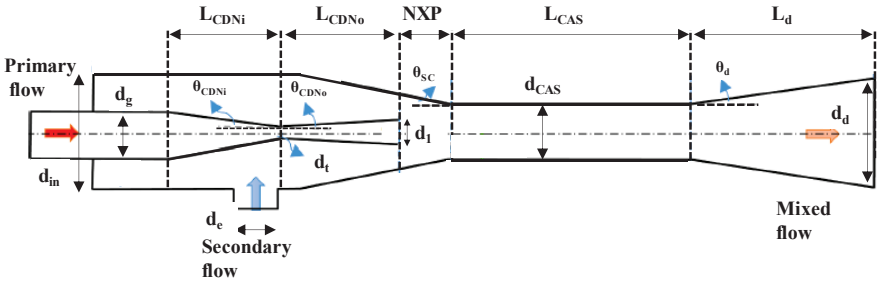

Figure 1: Ejector geometric parameters

The values of all geometric parameters of the ejector are summarized in Table 2. As it was previously mentioned, two ejector geometries are considered. These two geometries have the same parameters except for the NXP; in the first ejector geometry, it is equal to 25.20 mm, while in the second ejector geometry, it is equal to 16.80 mm.

Table 2 Ejector main geometrical parameters

Converging-diverging nozzle dimensions	
d_g (mm)	8.00
d_e (mm)	16.92
d_t (mm)	2.90

https://doi.org/10.52202/077185-0166

d_l (mm)	5.20
θ_{CDNi}(°)	12.00
θ_{CDNo}(°)	4.00
L_{CDNi}(mm)	11.99
L_{CDNo} (mm)	16.45
θ_{sc}(°)	30.00
NXP (mm)	25.20 (Ejector 1), 16.80 (Ejector 2)
d_{in} (mm)	27.99
Constant area section dimensions	
d_{CAS} (mm)	8.6
d_d (mm)	18.2
θ_d (°)	3.5
L_{CAS} (mm)	68.8
L_d(mm)	78.8

2.3 1-D ejector modeling approach

The 1-D modelling approach is based on the model developed by Huang et al. (Huang et al., 1999). The 1-D model is described in detail in the aforementioned publication, so the reader is prompted to it for more in depth analysis of the model and a presentation of the calculation method and used equations. In the present study, only essential information is presented. The model is developed in Matlab(Matlab, 2012), while working fluid properties are calculated with REFPROP (Huber, Lemmon, Bell, & McLinden, 2022).

Overall, the 1-D ejector model employs ideal gas laws and includes a set of empirical parameters. Two of these are the primary flow compression isentropic efficiency at the CDN ($\eta_p = 0.95$) and the secondary flow compression isentropic efficiency ($\eta_s = 0.85$). Two additional parameters include the CAS area correction factor (φ_p) and the mixing efficiency (φ_{mix}). These are strongly dependent on the ejector geometry, the operating conditions and the working fluid, with several empirical correlations having been proposed in different studies. Mwesigye and Dworkin (Mwesigye & Dworkin, 2018) combined the correlations that had been developed based on experimental results for working fluids R141b (Huang et al., 1999) and R245fa (Shestopalov et al., 2015) and derived the following generalized correlations, which have been used in the present work:

$$\varphi_p = 1.139 + 0.01768\frac{A_{CAS}}{A_t} - 0.009797\frac{p_p}{p_s} - 1.08\tilde{R} \quad (2)$$

$$\varphi_{mix} = 0.8264 - 0.01254\frac{A_{CAS}}{A_t} + 0.005804\frac{p_p}{p_s} + 0.4589\tilde{R} \quad (3)$$

The original ejector model as formulated in the study by Huang et al. (Huang et al., 1999) is more "rating-oriented", thus it is used for predicting the secondary mass flow rate, entrainment ratio and backpressure of an ejector of a known geometry, when the pressure and temperature of the primary and secondary flows are known. For the design of the ejector, the original model was modified and turned into a "design-oriented" sizing model, which is used for determining the dimensions of the ejector. In this case, the primary and secondary flow states at the ejector inlet are known, along with the primary flow mass flow rate and ejector backpressure, the latter mirroring (but not being identical to, as it will be later explained) the condensation pressure dictated by the cycle design. The inputs and outputs of the ejector model used for "rating" and "design" are summarized in Table 3.

Table 3 Ejector model inputs and outputs

Ejector "design" model (geometry to be specified)	
Inputs	**Outputs**
Primary flow mass flow rate, pressure and temperature	Secondary flow mass flow rate
Secondary flow pressure and temperature	entrainment ratio
Ejector backpressure	Ejector main dimensions (d_t, d_{CAS})
Ejector "rating" model (geometry is specified a priori)	

 https://doi.org/10.52202/077185-0166

Inputs	**Outputs**
Ejector main dimensions ($d_{t,}d_{CAS}$)	Primary flow mass flow rate
Primary flow pressure and temperature	Secondary flow mass flow rate
Secondary flow pressure and temperature	ejector backpressure
	entrainment ratio

The operation of ejectors of a given geometry is commonly expressed in the diagram by Huang et al. (Huang et al., 1999), shown in Figure 2, which correlates the entrainment ratio with the ejector backpressure.

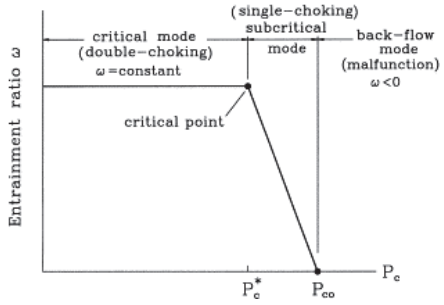

Figure 2: Entrainment ratio vs ejector backpressure(Huang et al., 1999)

Depending on the backpressure, three operating modes are distinguished. In the first mode (critical mode), in which both the primary and the secondary flows are chocked, the backpressure does not affect the entrainment ratio and the ejector operates as intended, as the mass flow rates of both the primary and secondary streams are maximized (being choked). If the backpressure surpasses a certain value (P_c*), only the primary flow is chocked (subcritical mode). In this case, the entrainment ratio exhibits a linear decline as the backpressure increases and the ejector operates sub-optimally. Finally, if the backpressure exceeds another value, called critical backpressure (P_{co}), the secondary flow is reversed (back-flow mode) and the ejector malfunctions.

If ideal conditions (i.e. no pressure drop in the ECC circuit) are assumed, the ejector backpressure is equal to the condensation pressure. However, this is not the case in real conditions, in which significant pressure losses may occur. Therefore, to ensure the operational feasibility of the ECC prototype, the design ejector backpressure has been taken equal to the condensation pressure increased by about 0.8 bar. This design decision results in lower ejector performance but ensures its operation feasibility throughout the demonstration campaign of the prototype. According to the simulation results obtained by the 1-D model, under these conditions, the secondary flow mass flow rate is equal to about 0.0062 kg/s, while the entrainment ratio is about 0.135. Finally, the ejector critical backpressure is 3.16 bar, corresponding to a saturation condensation temperature of around 52.5°C. Note that for lower condensation pressures, the mass flow rate of the secondary flow and thus the ejector entrainment ratio is the same (as shown in Figure 2).

2.4 Description of 2-D CFD models

A computational model of the ejector was developed and simulated using the Finite Volume Method (FVM) in ANSYS Fluent software. To reduce the computational costs which a full 3-D model would entail, 2-D models were created (pure 2-D and axisymmetric), which still captured all the necessary features of the ejector while maintaining a reasonable level of detail. The model included the convergent-divergent nozzle, which delivers the primary flow to the suction chamber, the inlet of the secondary flow, the cylindrical mixing chamber, and the diffuser. Two different geometries were compared, both including the same features but varying only in terms of nozzle exit position (often termed as NXP). The first model had an NXP value of 25.20 mm, while the second model had an NXP value of 16.80 mm. This allows for a comparison of the effects of different nozzle exit positions on the performance of the ejector and especially the entrainment ratio.

The computational grid consisted of 123040 quadrilateral cells in the first model and 118979 quadrilateral cells in the second model, with an average element quality of 0.96114 and 0.96401,

https://doi.org/10.52202/077185-0166

respectively. In the case of the axisymmetric model, half of the original computational domain was included but the resulting mesh had the same cell size as the pure 2-D model.
The boundary conditions were defined to accurately simulate the behavior of the ejector. The inlet of the primary flow was set to a pressure value of 17.35 bar and a temperature of 403 K (130°C). Moreover, the inlet of the secondary flow was set to a pressure value of 0.65 bar and a temperature of 285 K (12°C), whereas the outlet was set to a pressure value of 2.35 bar. The other boundaries were assumed to be rigid walls with no slip conditions for the fluid flow and adiabatic boundary conditions for temperature. In the axisymmetric model, symmetry boundary conditions were imposed on the axis of the ejector. Gravity was taken into account with an acceleration value equal to 9.81 m/s^2.
The fluid flow was simulated by solving the continuity and momentum differential equations in 2-D and given that the fluid is considered compressible, the heat transfer differential equation was also solved in the computational domain. Moreover, due to particularities of the flow in the ejector, such as high velocities (high Reynolds number) and high pressure gradients, the effect of turbulence should be also taken into account. In this work, the standard k-ε 2 equation turbulence model was employed with scalable wall functions and including compressibility effects, due to the anticipated transonic and supersonic flow in several parts of the ejector.
In order to compare the outcome of the 2-D CFD models with the 1-D model, it was decided to use the same values for thermophysical properties. The working fluid, R1233zd(E), was assumed to be a single phase ideal gas, and its thermophysical properties were obtained using thermodynamics software (REFPROP, as mentioned before). These properties were considered constant and equal to the arithmetic average of the properties at two different operating points: one representing the conditions at the inlet of the primary flow and the other representing the conditions at the inlet of the secondary flow. Thus, specific heat (c_p) was assumed equal to 1038.595 J/kg K, thermal conductivity (k) equal to 0.015515 W/mK, viscosity(μ_{visc}) equal to 1.3394 10^{-5}Pa*s, and molecular weight (M_w) equal to 130.5 kg/kgmol.
For the solution, a pressure-based solver was employed with double precision calculations, and a steady-state approach was adopted. In each case, the solution was obtained after 20000 iterations, as it was observed from the residuals' graph that this was a sufficient number of iterations for flow and thermal phenomena to converge. It is worth noting that, especially in the 2-D axisymmetric model, the mass flow rate values converge after less than 1000 iterations, but the flow field characteristics were stabilized after a longer time.

3 RESULTS

A comparative overview of the velocity contours for the two ejector geometries as computed by the CFD pure 2-D model for the evaluated NXP values is illustrated in the diagrams of Figure 3. Overall, the flow field is similar for both investigated NXP values. While the flow is mostly symmetrical inside the CDN, it is non-symmetrical from the mixing section to the outlet (diffuser) of the ejector. The reason for this asymmetry is likely the fact that the secondary flow enters the ejector device non-symmetrically, since the low-pressure inlet port is located at the bottom. Notably, for the ejector featuring a smaller NXP, the supersonic jet core extends even further into the mixing section. Overall, from a qualitative perspective, the results are compatible with theoretical and experimental results that have been reported in the literature.

https://doi.org/10.52202/077185-0166

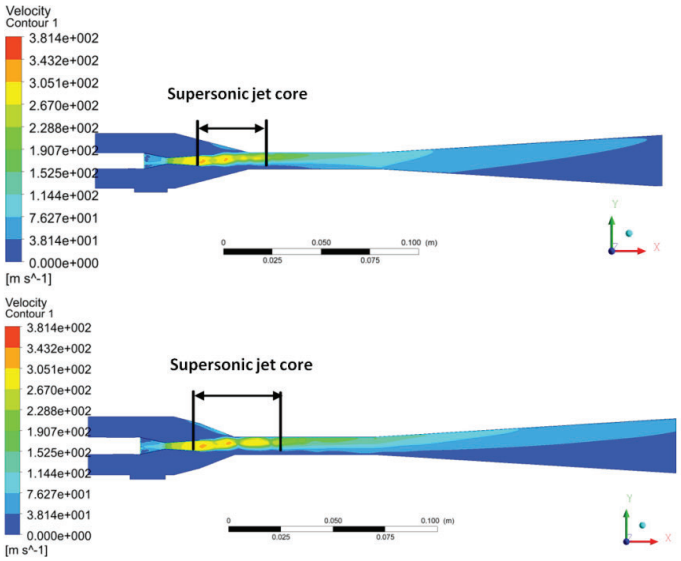

Figure 3: Velocity field (pure 2-D) for NXP=25.20 mm (top) and NXP=16.80 mm (bottom)

More specifically, in both cases, the primary flow is accelerated in the converging section of the CDN, attaining sonic speed (M=1) at the CDN throat and being further accelerated to supersonic speeds at the CDN diverging section, as shown in more detail in Figure 4.

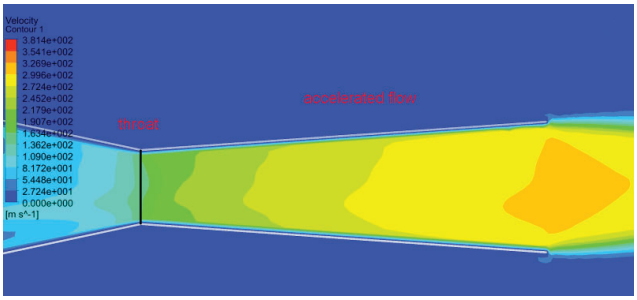

Figure 4: Velocity field inside the CDN, before and after the throat region (NXP=25.20 mm)

As shown in **Figure 5**, in the mixing section after the CDN, the secondary flow restricts the flow area available for the supersonic primary flow, resulting in its deceleration. At the same time, the subsonic secondary flow is accelerated and becomes sonic, being gradually mixed with the primary flow after their pressures are equalized. The development of shock structures indicated by the formation of shear layers in the primary flow after the exit of the CDN is observed near the exit of the suction chamber and the initial part of the mixing section. The length of the potential core of the primary flow (supersonic jet core) extends up to more than 10 mm into the mixing section, especially for the ejector with NXP = 16.80 mm, whereas the velocities rapidly decrease towards the end of the mixing section and the diffuser. In the diffuser, the mixed flow is decelerated as the pressure increases, being ultimately equalized to the backpressure at the exit of the diffuser (Shi et al., 2015).

https://doi.org/10.52202/077185-0166

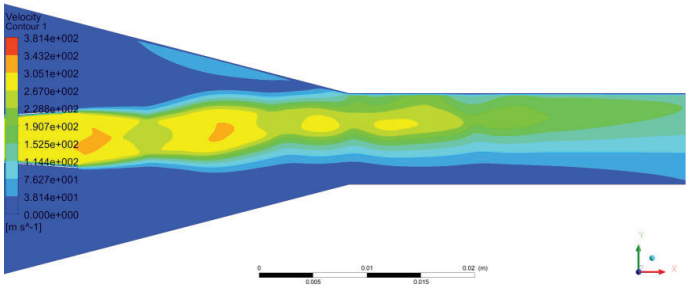

(a)

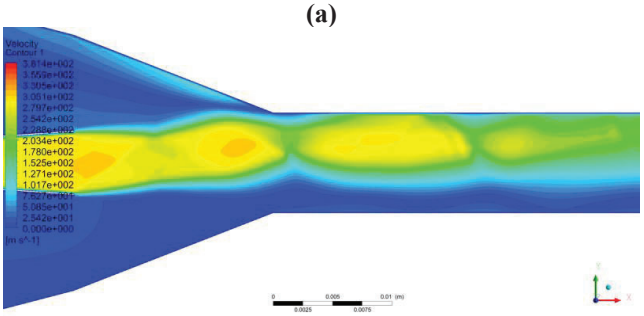

(b)

Figure 5: Velocity field after the nozzle until the initial region of the mixing section: (a) NXP = 25.20 mm, (b) NXP = 16.80 mm

In the case of the 2-D axisymmetric model, as it can be seen in Figure 6, the velocity distribution is obviously symmetric with higher velocities closer to the axis of the ejector and lower towards the walls. The flow is accelerated after the throat of the CDN and when the working medium reaches the end of the constant area section, velocity is considerably reduced to the recovery of pressure in the diffuser. Contrary to the case of the pure 2-D model, no significant differences are observed in the case of different NXP value, something that will be reflected in the mass flow rate and entrainment results afterwards. Although the magnitude of velocities is similar for both pure 2-D and axisymmetric 2-D models, the representation of the flow structures inside the ejector differs in several areas. Although the formation of shock structures after the CDN towards the end of the suction chamber is again visible, the boundary and subsequent layers appear in a more gradual succession and no divergence of the flow towards the walls in the diffuser section is predicted.

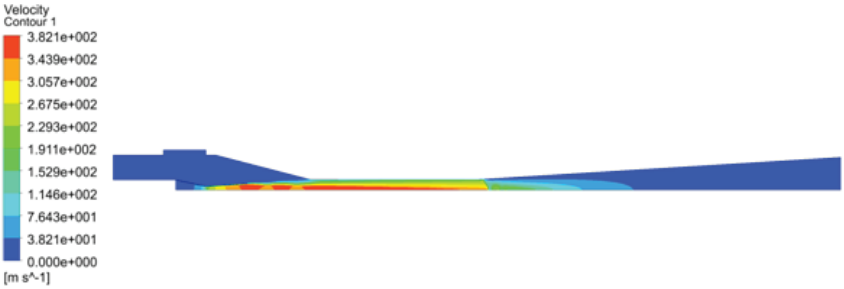

(a)

https://doi.org/10.52202/077185-0166

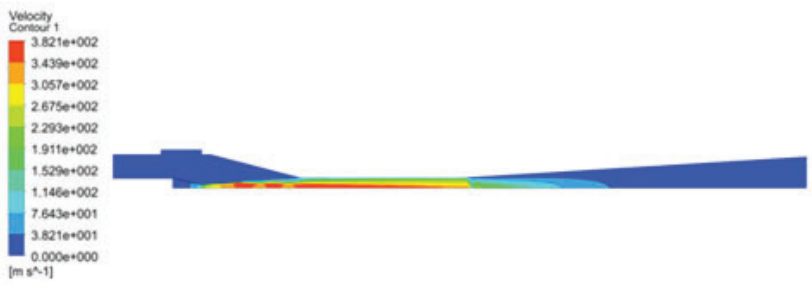

(b)

Figure 6: Velocity field (axisymmetric) for (a) NXP=16.80 mm and (b) NXP=25.20 mm

According to the pure 2-D CFD model, the mass flow rate of the inlet of the primary flow was estimated at 0.0483 kg/s for the first and 0.0480 kg/s for the second geometry, respectively, whereas the respective values for the mass flow rate of the secondary flow were 0.0163 kg/s and 0.0127 kg/s. Therefore, the entrainment ratio corresponding to the two geometries are equal to 0.3376 and 0.2646, respectively. Thus, the results from the pure 2-D CFD model suggest that the decrease of the NXP by 8.4 mm leads to a decrease of both secondary inlet flow and entrainment ratio. For the selected range of NXP values, the preliminary results of the pure 2-D CFD model revealed that an improvement of the entrainment ratio and subsequently the ejector performance can be performed by appropriately adjusting the NXP. On the other hand, as can be seen in Table 4, the results of the 2-D axisymmetric model indicate that the secondary inlet mass flow rate is much lower, as well as the entrainment ratio, whereas the change of NXP parameter plays a definitely less significant role. These results of the preliminary evaluation of the prototype imply that a more comprehensive study is needed for determining in detail the impact of the NXP on the ejector performance. Compared to the results of the 1-D model, which cannot take into account the different NXP values (Table 4), the value of predicted primary inlet mass flow rate is considerably close for both 2-D models, with a very small difference in the case of both ejector geometries (the relative deviation being equal to 0.65-6.37%). However, a large deviation is observed in the case of the mass flow rate of the secondary flow and hence the entrainment ratio. In particular, the secondary flow mass flow rate is almost 2.5 times in the case with NXP value of 25.20 mm while in the second case the difference is almost twofold. Notably, this difference also occurs for the axisymmetric model, although to a significantly lesser degree. The observed differences between 1-D and 2-D CFD models can be attributed to the fact that flow-related properties such as viscosity or the effect of turbulence (Grazzini, Milazzo, & Mazzelli, 2018; Xiao et al., 2022) is not directly taken into account in the 1-D model except for some specialized coefficients for component efficiency, whereas the solution of the 2-D CFD models depends significantly on these factors, apart from the thermodynamic properties of the working fluid.

Table 4 Comparative evaluation of 1-D and 2-D CFD models results

Parameter	1-D model	Pure 2-D CFD (NXP=25.20 mm)	Pure 2-D CFD (NXP=16.80 mm)	Axisymmetric 2-D CFD (NXP=25.20 mm)	Axisymmetric 2-D CFD (NXP=16.80 mm)
$\dot{m}_p$ (kg/s)	0.0455	0.0484 (+6.37%)	0.0480 (+5.49%)	0.0458 (+0.65%)	0.0459 (+0.88%)
$\dot{m}_s$ (kg/s)	0.0062	0.0163(+162.90%)	0.0127(+104.84%)	0.0034 (-45.16%)	0.0035 (-43.55%)
ω (-)	0.1354	0.3376(+149.34%)	0.2645(+95.35%)	0.0742 (-45.19%)	0.0763 (-43.65%)

4 CONCLUSIONS

A theoretical preliminary investigation was conducted to evaluate the performance of an ejector device using two computational methods: a 1-D model and 2-D CFD models.
In this study, it was found that the 2-D CFD models provided a more detailed understanding of fluid flow inside the ejector, including velocity and pressure fields, subsonic and supersonic flow transitions, and shock structures.

https://doi.org/10.52202/077185-0166

The pure 2-D CFD model showed that changing the nozzle exit position value affected the mass flow rate of the secondary flow and entrainment ratio. However, models with different NXP shared similar velocity and pressure fields, except for the mixing section, where shock structures were observed more prominently at lower nozzle exit positions. On the other hand, the 2-D axisymmetric model showed subtle differences between the two geometries and considerably lower secondary inlet mass flow rate and entrainment ratio from the pure 2-D model.

The comparison between the two types of models revealed significant deviations. The pure 2-D model overestimated the mass flow rate of the secondary flow and entrainment ratio compared to the 1-D model whereas the 2-D axisymmetric model moderately underestimated these quantities compared to the 1-D model. Therefore, appropriate adjustments to the 1-D model coefficients are necessary to improve its accuracy and further validation of the CFD models is required in order to reach a definite decision about the most appropriate model. In a future study the validation of all models will be performed by means of direct experimental measurements in the actual facility, in order to further evaluate the findings of this work.

NOMENCLATURE

Abbreviations

CAS	ejector Constant Area Section
CDN	Converging-diverging nozzle
CFD	Computational Fluid Dynamics
COP	Coefficient of Performance
ECC	Ejector Cooling Cycle
EVCC	Ejector-Vapor Compression Cycle
FVM	Finite Volumes Method
NXP	Nozzle Exit Position
WHR	Waste Heat Recovery

Greek characters

η	efficiency (isentropic)	(-)
μ	dynamic viscosity	(Pas)
ω	entrainment ratio	(-)
φ	efficiency (mixing or area correction factor)	(-)

Variables

A	cross sectional flow area	(m^2)
c	specific heat capacity	(kJ/kgK)
k	thermal conductivity	(W/mK)
M	Mach number	(-)
$\dot{m}$	mass flow rate	kg/s
M_w	molecular weight	kg/kmol
p	pressure	(bar)
$\tilde{R}$	ratio of working fluid gas constant divided by global gas constant	(-)

Subscripts

1	ejector CDN outlet
CAS	constant area section of ejector
CDNi	converging-diverging nozzle inlet
CDNo	converging-diverging nozzle outlet
d	diffuser
e	ejector low-pressure port
g	ejector high-pressure port

https://doi.org/10.52202/077185-0166

in	inlet
mix	mixing
out	outlet
p	constant-pressure, primary flow
s	secondary flow
t	CDN throat
w	weight (molecular)

ACKNOWLEDGEMENT

The work has been conducted as part of the ZHENIT project, that has received funding from the European Union's Horizon Europe research and innovation programme under grant agreement No 101056801.
The information presented on this document reflects only the authors' view. The Agency is not responsible for any use that may be made of the information it contains

REFERENCES

Besagni, G., Mereu, R., Chiesa, P., & Inzoli, F. (2015). An Integrated Lumped Parameter-CFD approach for off-design ejector performance evaluation. *Energy Conversion and Management, 105*, 697-715. doi:https://doi.org/10.1016/j.enconman.2015.08.029

Besagni, G., Mereu, R., & Inzoli, F. (2016). Ejector refrigeration: A comprehensive review. *Renewable and Sustainable Energy Reviews, 53*, 373-407. doi:https://doi.org/10.1016/j.rser.2015.08.059

Braimakis, K. (2021). Solar ejector cooling systems: A review. *Renewable Energy, 164*, 566-602. doi:https://doi.org/10.1016/j.renene.2020.09.079

Chen, Z., Jin, X., Shimizu, A., Hihara, E., & Dang, C. (2017). Effects of the nozzle configuration on solar-powered variable geometry ejectors. *Solar Energy, 150*, 275-286. doi:https://doi.org/10.1016/j.solener.2017.04.017

Croquer, S., Poncet, S., & Galanis, N. (2016). Comparison of ejector predicted performance by thermodynamic and CFD models. *International Journal of Refrigeration, 68*, 28-36. doi:https://doi.org/10.1016/j.ijrefrig.2016.04.026

Elbel, S., & Hrnjak, P. (2008). Ejector refrigeration: an overview of historical and present developments with an emphasis on air-conditioning applications.

ESDU. (1984). Ejector and Jet pumps, Design for Compressible Air Flow: ESDU 84029. *ESDU International Ltd, London, UK*.

ESDU. (1986). Ejector and Jet pumps, Design for Steam Driven flow: ESDU 862030. *ESDU International Ltd, London, UK*.

ESDU. (1992). Ejector and Jet pumps, Data Item: 92042. *ESDU International Ltd, London, UK*.

Grazzini, G., Milazzo, A., & Mazzelli, F. (2018). Ejector CFD Modeling. In G. Grazzini, A. Milazzo, & F. Mazzelli (Eds.), *Ejectors for Efficient Refrigeration: Design, Applications and Computational Fluid Dynamics* (pp. 117-150). Cham: Springer International Publishing.

Huang, B. J., Chang, J. M., Wang, C. P., & Petrenko, V. A. (1999). A 1-D analysis of ejector performance. *International Journal of Refrigeration, 22*(5), 354-364. doi:https://doi.org/10.1016/S0140-7007(99)00004-3

Huber, M. L., Lemmon, E. W., Bell, I. H., & McLinden, M. O. (2022). The NIST REFPROP database for highly accurate properties of industrially important fluids. *Industrial & Engineering Chemistry Research, 61*(42), 15449-15472.

Ma, X., Zhang, W., Li, F., & Riffat, S. B. (2019). Solar Ejector Cooling Technologies. In X. Zhao & X. Ma (Eds.), *Advanced Energy Efficiency Technologies for Solar Heating, Cooling and Power Generation* (pp. 287-309). Cham: Springer International Publishing.

Matlab, S. (2012). Matlab. *The MathWorks, Natick, MA*.

https://doi.org/10.52202/077185-0166

Mwesigye, A., & Dworkin, S. B. (2018). Performance analysis and optimization of an ejector refrigeration system using alternative working fluids under critical and subcritical operation modes. *Energy Conversion and Management, 176*, 209-226. doi:https://doi.org/10.1016/j.enconman.2018.09.021

Park, H., & Kang, S. H. (2023). Development of a 1D solution algorithm to predict ejector performance in high altitude wind tunnels. *Journal of Mechanical Science and Technology, 37*(11), 6037-6045.

Riffat, S., Jiang, L., & Gan, G. (2005). Recent development in ejector technology—a review. *International journal of ambient energy, 26*(1), 13-26.

Sanaye, S., Farvizi, A., Refahi, A., & Rafieinejad, M. V. (2019). A novel application of optimization and computational fluid dynamics methods for designing combined ejector-compressor refrigeration cycle. *International Journal of Refrigeration, 108*, 174-189. doi:https://doi.org/10.1016/j.ijrefrig.2019.06.006

Shestopalov, K. O., Huang, B. J., Petrenko, V. O., & Volovyk, O. S. (2015). Investigation of an experimental ejector refrigeration machine operating with refrigerant R245fa at design and off-design working conditions. Part 1. Theoretical analysis. *International Journal of Refrigeration, 55*, 201-211. doi:https://doi.org/10.1016/j.ijrefrig.2015.01.016

Shi, C., Chen, H., Chen, W., Zhang, S., Chong, D., & Yan, J. (2015). 1D Model to Predict Ejector Performance at Critical and Sub-critical Operation in the Refrigeration System. *Energy Procedia, 75*, 1477-1483. doi:https://doi.org/10.1016/j.egypro.2015.07.271

Song, Y., Ma, Y., Wang, H., Yin, X., & Cao, F. (2020). Review on the simulation models of the two-phase-ejector used in the transcritical carbon dioxide systems. *International Journal of Refrigeration, 119*, 434-447. doi:https://doi.org/10.1016/j.ijrefrig.2020.04.029

Tashtoush, B. M., Al-Nimr, M. d. A., & Khasawneh, M. A. (2019). A comprehensive review of ejector design, performance, and applications. *Applied Energy, 240*, 138-172. doi:https://doi.org/10.1016/j.apenergy.2019.01.185

Van den Berghe, J., Bartosiewicz, Y., & Mendez, M. A. (2023). *An overview on the development and calibration of a 1D ejector model.* Paper presented at the 14th Symposium of VKI PhD Research 2023.

Van den Berghe, J., Dias, B. R. B., Bartosiewicz, Y., & Mendez, M. A. (2023). A 1D model for the unsteady gas dynamics of ejectors. *Energy, 267*, 126551. doi:https://doi.org/10.1016/j.energy.2022.126551

Xiao, J., Wu, Q., Chen, L., Ke, W., Wu, C., Yang, X., . . . Jiang, H. (2022). Assessment of Different CFD Modeling and Solving Approaches for a Supersonic Steam Ejector Simulation. *Atmosphere, 13*(1), 144.

Yadav, S. K., Murari Pandey, K., & Gupta, R. (2021). Recent advances on principles of working of ejectors: A review. *Materials Today: Proceedings, 45*, 6298-6305. doi:https://doi.org/10.1016/j.matpr.2020.10.736

 https://doi.org/10.52202/077185-0166